Estuarine-deltaic controls on coastal carbon burial in the western Ganges-Brahmaputra delta over the last 5,000 years

R.P., Flood[1,*,†], M.G., Milne[2], G.T., Swindles[1,3], I.D., Barr[4], J.D., Orford[1]

[1]Geography, School of Natural and Built Environment, Queen's University Belfast, Belfast, BT7 1NN, UK

[2]Veterinary Sciences Division, Agri-food and Biosciences Institute (AFBI), 12 Stoney Road, Stormont, Belfast, BT4 3SD, UK

[3]Ottawa-Carleton Geoscience Centre and Department of Earth Sciences, Carleton University, Ottawa, Ontario, Canada

[4]Geography and Environmental Management, School of Science and the Environment, Manchester Metropolitan University, Manchester, UK

[*]Corresponding author e-mail address: *rory.p.flood@gmail.com*

[†]No longer at this institution where the research was carried out.

Estuarine-deltaic controls on coastal carbon burial in the western Ganges-Brahmaputra delta over the last 5,000 years

R.P., Flood[1,*,†], M.G., Milne[2], G.T., Swindles[1,3], I.D., Barr[4], J.D., Orford[1]

[1]Geography, School of Natural and Built Environment, Queen's University Belfast, Belfast, BT7 1NN, UK

[2]Veterinary Sciences Division, Agri-food and Biosciences Institute (AFBI), 12 Stoney Road, Stormont, Belfast, BT4 3SD, UK

[3]Ottawa-Carleton Geoscience Centre and Department of Earth Sciences, Carleton University, Ottawa, Ontario, Canada

[4]Geography and Environmental Management, School of Science and the Environment, Manchester Metropolitan University, Manchester, UK

[*]Corresponding author e-mail address: rory.p.flood@gmail.com

[†]No longer at this institution where the work was carried out.

Keywords: Ganges-Brahmaputra delta; carbon; carbon burial; sedimentation; Sundarbans; beta regression.

Abstract

The Ganges–Brahmaputra fluvial system drains the Himalayas and is one of the largest sources of terrestrial biosphere carbon to the ocean. It represents a major continental reservoir of CO_2 associated with c. 1–2 billion tons of sediment transported each year. Shallow coastal environments receive substantial inputs of terrestrial carbon (900 Tg C yr^{-1}), with allochthonous carbon capture on connected floodplains. Vegetated coastal ecosystems play a dominant role in the sequestration of carbon and operate as highly efficient carbon sinks. Mangrove sediments are subject to intense carbon-fixing processes that have a potentially high impact on the global carbon budget. The Sundarbans is the largest tidal mangrove forest in the world (10,200 km^2 in area) and is located on the marine-terrestrial boundary of the Ganges-Brahmaputra delta and the Bay of Bengal, in West Bengal (India) and Bangladesh. Estimates of sedimentation on the tidal delta plain of the Ganges-Brahmaputra delta reveal mean rates of $\sim$1.1 cm yr^{-1} with accretion understood to approximately equal the regional rate of sea-level rise of $\sim$1.0 cm yr^{-1}. In this study, the properties of sediments from the western Ganges-Brahmaputra delta are used to investigate controls on coastal carbon burial over the past 5,000 years. Our main findings are: (1) Beta regression of aluminium and silica ratio data is a robust method of estimating total organic carbon in sediment from the Indian Sundarbans; (2) the estimated rate of sediment deposition over last 5,000 years is between 1.0 and 2.5 mm yr^{-1}, with uncertainty surrounding the reworked origins of sediment; and (3) temporal variation of total organic carbon accumulation through the last 5,000 years is generated by varying sedimentary depositional processes. The delivery and burial of total organic carbon is predicated on the continual supply of sediment to the Sundarbans, which future management strategies may need to consider given changing rates of deposition.

1. Introduction

The world's oceans absorb atmospheric carbon dioxide (CO_2) at a rate comparable to that of terrestrial ecosystems (Stocker et al., 2013; Watanabe and Kuwae, 2015). Coastal systems are the interface between the land and the ocean and can act as carbon reactors that store, process, and emit organic carbon (OC) (Butman et al., 2016; Galy et al., 2015, 2007; Hotchkiss et al., 2015; Luisetti et al., 2019; Scott and Wohl, 2017; Sutfin et al., 2016). There is now widespread recognition (Luisetti et al., 2019) that coastal environments themselves (e.g., mangroves, saltmarshes, and seagrass ecosystems) represent major globally-important carbon sinks and stores (i.e., "Blue Carbon").

In estuarine coastal systems, the rate of OC burial is estimated to be higher (238 Tg C yr^{-1}) than in the open ocean (6 Tg C yr^{-1}) (Nellemann et al., 2009; Watanabe and Kuwae, 2015). Shallow coastal environments also receive a substantial input of terrestrial carbon (C)

(900 Tg C yr^{-1}), with allochthonous carbon capture on floodplains (Regnier et al., 2013). Vegetated coastal ecosystems play a key role in the sequestration of carbon particularly in sea-grass meadows, mangrove forests, and tidal salt marshes as highly efficient C sinks (Alongi, 2012; Bouillon et al., 2008; Bu et al., 2015; Chmura et al., 2003; Duarte et al., 2010, 2005; Iacono et al., 2008; Kennedy et al., 2010; Laffoley et al., 2009; Luisetti et al., 2019; Mcleod et al., 2011; Nellemann et al., 2009). In such vegetated coastal ecosystems, long-term Holocene (c. 8 – 10 ka years) rates of C accumulation in sediments range between 18 and 1713 g C m^{-2} yr^{-1} (Mcleod et al., 2011). In comparison long-term Holocene rates of C accumulation in soils of temperate, tropical, and boreal forests range only between 0.7 and 13.1 g C m^{-2} yr^{-1} (Mcleod et al., 2011), emphasising the importance coastal ecosystems may have for the sensitivity of contemporary and future C sequestration and the Earth's C cycle more generally.

The Ganges–Brahmaputra (G–B) system drains the Himalayas and is one of the largest sources of terrestrial biospheric carbon to the ocean. It therefore represents a major continental reservoir of CO_2 (Galy et al., 2008; Galy and Eglinton, 2011). Approximately 1–2 billion tons of sediment are transported each year by the G–B fluvial system from the Himalayas to the Bay of Bengal, with final deposition in the Bengal Fan (Galy et al., 2008). Fluvial sedimentary characterisations of OC flux have the global significance of modern river sources (Aucour et al., 2006; France-Lanord and Derry, 1997; Galy et al., 2008; Subramanian and Ittekot, 1991). In the Bengal Fan, modern burial flux of recent OC generated by Himalayan erosion is $3.1 \pm 0.3 \times 10^{11}$ mol yr^{-1} (Galy et al., 2008, 2007). This flux of OC represents c. 15% of the global OC flux (Galy et al., 2008, 2007). OC burial in the Himalayan system is extremely efficient, with nearly 100% of the OC exported by the G–B fluvial system buried in Bengal Fan sediments (Galy et al., 2008). Thus, the G–B fluvial system plays a significant role in the effective transport and burial of OC, which has major implications for atmospheric CO_2 sequestration (Galy et al., 2008).

Deltaic wetlands consist of one of the most dynamic landscapes and are under threat by relative sea-level rise (RSLR) and decreases in fluvial sediment supply (Wagner et al., 2017; Yang et al., 2020). The role of wetlands, particularly tidal wetlands, in carbon sequestration is well recognised with the possibility of incorporating carbon credits for tidal wetland restoration into the development of both voluntary and regulatory carbon markets for atmospheric CO_2 emissions reductions (Callaway et al., 2012; Crooks et al., 2010; Freedman et al., 2009; Hansen, 2009; Laffoley et al., 2009). Restoration of wetlands and ecosystem function could be tied with carbon credits in order to bury carbon (Callaway et al., 2012; Emmett-Mattox et al., 2011). The viable function of a carbon credit system would be primarily on the basis that approximately 100 years' worth of carbon could be buried, without the potential of carbon decomposition and return to the atmosphere (Callaway et al., 2012; Crooks et al., 2010). Determination of TOC burial in wetlands, particularly where restoration efforts have taken place, need baseline estimates of TOC to judge the efficacy of restoration and TOC burial (*cf.,* Callaway et al., 2012). The Indian Sundarbans offers a unique site to study burial of TOC over centennial to millennial timescales. The primary aim of this study is to quantify TOC in the Indian Sundarbans and examine the relationship between sedimentary processes in the accumulation of TOC.

2. Materials and methods

2.1. Study Site

The Sundarbans, split between India and Bangladesh (Fig. 1), is the largest tidal mangrove forest in the world at 10,200 km^2. It is located on the marine-terrestrial boundary of the G-B delta and the Bay of Bengal (Dutta et al., 2017). The Sundarbans was established as a UNESCO world heritage reserve site, with 60% of the reserved forest located in Bangladesh, and 40% in India (Dutta et al., 2017). The Indian Sundarbans Biosphere Reserve (SBR), an area of c. 9,600 km^2, involves 1,800 km^2 of estuarine channels and 3,600 km^2 of reclaimed areas (Dutta et al., 2017). The Indian Sundarbans is dominated by a series of north-south oriented estuarine tidal channels (i.e., the Mooriganga, Saptamukhi, Thakuran, Matla, Bidya, Gosaba, and Haribhanga), which define an archipelago of 102 islands, with 54 having been reclaimed for human settlement and the remainder uninhabited (Dutta et al., 2017). The overall morphology of the Sundarbans indicates a west to east continuum of tidal, mixed tidal-fluvial, and predominantly fluvial sedimentary processes operate (Flood et al., 2018; Rogers et al., 2013). The overall G-B delta is divided into two key systems, the older fluvially-abandoned part in the west, now tidally-dominated (the focus of this study), and the eastern, fluvially-dominated system, with associated fluvially-driven shoreline progradation following the joining of the Ganges and Brahmaputra Rivers (Allison, 1998a; Flood et al., 2018; Rogers et al., 2013). The western extent of the delta, that underlies the present day Indian Sundarbans, was fluvially abandoned prior to c. 5000 cal years BP, with the migration of the Ganges River eastward towards its present position (Flood et al., 2018; Goodbred and Kuehl, 2000; Rogers et al., 2013; Sarkar et al., 2009). Since this eastern migration of the Ganges, the Indian Sundarbans is considered to have been principally estuary-tidal dominated.

2.2. Sediment coring

The study site is shown in Fig. 1, with an inlay map showing the extent of the West Bengal Sundarbans. The primary surface sedimentary unit under investigation for TOC is the thin mud facies (TMF); understood to be a Late Holocene (c. 5000 cal years BP to present) capping unit of the Quaternary stratigraphy (Goodbred and Kuehl, 2000). The TMF consists of overbank deposits of the modern and recent floodplain system, found in floodplain environments and is absent near active fluvial channels (Goodbred and Kuehl, 2000). Coring of the TMF sediment was conducted using a motor driven percussion coring device, with latitude, longitude and elevation recorded with a differential GPS. Shallow percussion coring was conducted at Lothian, Gplot, Dhanchi (2010), and Dhanchi-2, Bonnie Camp, and Sajnekhali (2011) sites (Fig. 1). A detailed summary of these sites is provided in Flood (2014) and Flood et al. (2018, 2016).

2.3. ED-XRF geochemistry of the Sundarbans

Data acquisition using energy dispersive – X-ray fluorescence spectrometry (ED-XRF) was undertaken following the approach outlined by Flood et al. (2018, 2016), using a Bruker S1 TURBO SD portable X-ray fluorescence (PXRF) spectrometer (Bruker Corporation, Massachusetts, USA) consisting of a 10 mm X-Flash® SDD Peltier-cooled detector with a 4-W X-ray tube with an Ag target and a maximum voltage of 40 kV. Analysis was performed on discrete samples collected from the Lothian, Gplot, Dhanchi, Dhanchi-2, Bonnie Camp, and Sajnekhali Island cores. Precision and accuracy of the preparation and the instrumental performance of the PXRF was checked using the international reference samples and a summary of these is provided by (Flood et al., 2016). Al and Si values were log-normal (ln) transformed for the purposes of TOC prediction using binomial logistic and beta regression model coefficients.

2.4. Development of TOC prediction for the Ganges-Brahmaputra Delta: modelling approaches used

There is a monotonic and simultaneous relationship between sediment properties and OC in the G-B as identified by Galy et al. (Galy et al., 2015, 2011, 2008, 2007) and is understood to result from OC content that is (1) mainly controlled by sediment properties, and/or (2) affected by mixing and sorting processes, akin to mixing and sorting of detrital grains. Two species modes of OC have been identified in the sediments of the G-B river and delta: (1) organomineral associations; and (2) free organic particles. Within suspended sediments of the G-B system, there is a tendency for segregation of free organic particles by size, in a similar manner to detrital mineral grains; with fine grained sediments hosting mainly tiny free organic particles, and coarse sediments hosting coarse organic debris. The most significant relationship between sediment properties and TOC has been found by Galy et al. (2007), who identified a high degree of correlation between TOC and the aluminium to silica (Al/Si) ratio (Supplementary Figure B1). The Al/Si ratio represents the bulk mineralogical composition of the sediments being a proxy for sediment size; low Al/Si values indicate high proportions of quartz and low TOC, while high Al/Si indicate high proportions of micas and clay minerals, and higher TOC (Galy et al., 2011, 2007).

2.5. Estimation of TOC from Al/Si – the beta regression modelling approach

The ultimate aim of this component of the analysis was to use the previously published TOC and Al/Si ratio data by Galy et al. (2007) as a calibration dataset to derive estimates of TOC values for the six sites in Figure 1. The Galy et al. (2007) data were selected for this purpose based on both location relative to potential sediment inputs from the Ganges-Brahmaputra-Meghna river systems; along with these samples being retrieved from contemporaneous sediments of the TMF unit. This was achieved by fitting the original model between Al/Si and TOC from Galy et al. (2007), and using this model to "predict" TOC at our six sites of interest.

Linear regression models using ordinary least squares (OLS) and maximum likelihood estimation (MLE) are a generally accepted approaches used to examine the relationship between an independent (predictor) variable and a dependent (outcome / response) variable. However, these models pose serious challenges and are found to be inappropriate where the response variable is restricted to the interval (0, 1); i.e., where the response variable is constrained by a unit sum (Douma and Weedon, 2019; Ferrari and Cribari-Neto, 2004; Weltje and Tjallingii, 2008). As a result of this imposed constraint, OLS estimation may yield fitted values for the variable of interest that exceed both lower and upper bounds, and in some cases produce values greater than 1, and <0, which is especially profound in cases where measurements are low (Ferrari and Cribari-Neto, 2004; Weltje and Tjallingii, 2008). As a result, where there may be a high degree of goodness-of-fit (e.g., $R^2 = 0.99$), such linear relations are unlikely to be applicable outside the range of variation of the samples on which they are based (Weltje and Tjallingii, 2008).

A common solution to these challenges include transformation of the dependent variable so that data assumes values in real Euclidean space ($\mathbb{R}^n$), and then to model the mean of the transformed response as a linear predictor. A number of issues are encountered with this transformation approach, principally the fact that the model parameters cannot be easily interpreted in terms of the original response. A better approach requires the use of generalised linear models (GLMs) which are mathematical extensions of linear models that allow for outcome data to vary from normality constraints (e.g., outcome data can assume binomial, Poisson, negative binomial, or gamma distribution) (Guisan et al., 2002). In this instance, the binomial model was used to model outcomes which vary between 0 and 1, but with the limitation that such models are usually more applicable for modelling fractional counts e.g. 1/5, 2/5. TOC data, however, is continuous and thus represents a "true" proportion e.g. "20%", as opposed to a fractional proportion. Beta regression (Douma and Weedon, 2019; Ferrari and Cribari-Neto, 2004) provides some additional flexibility to model these types of data. Furthermore, measures of proportions are generally asymmetric, and inferences based on the normality assumption can be misleading as a result (Ferrari and Cribari-Neto, 2004) making the beta distribution more appropriate for these data. TOC was reported as a percentage, but was easily converted into proportions (prop.) by dividing by 100 prior to modelling. Whilst we fit the Galy et al. (2007) data using the binomial distribution and beta distribution, the primary focus of this work are models fitted using the beta distribution, and the majority of the results will refer to this. The binomial models are, however, presented for the sake of comparison.

Binomial logistic regression was carried out using the 'stats' package in R Version 4.1.2 (Core Team, 2021), with a logistic link function and the binomial model family. Beta regression was carried out using the 'betareg' package by (Cribari-Neto and Zeileis, 2010) in R Version 4.1.2 (Core Team, 2021). Linear regression of predicted TOC against depth, along with graphical illustration of binomial logistic regression and beta regression results was carried out using the 'ggplot2' package (Wickham, 2016) in R Version 4.1.2 (Core Team, 2021).

2.6. Grain size analysis

Given the importance of the Al/Si ratio for determination of TOC, and given the relationship between sediment properties and/or mixing and sorting processes, grain-size distributions (GSDs) from the West Bengal Sundarbans were analysed following Flood et al. (2016, 2015, 2018) using a Malvern Mastersizer 2000™ instrument. Zeros were replaced with a small constant (0.001), with a sensitivity analysis carried out against other small constants (i.e., 0.01 and 0.1) showing no discernible variation in median grain-size (i.e., D_{50} μm). GRADISTAT software was used for the analysis of grain-size data in order to calculate grain size statistical parameters, with median grain-size in microns (μm), and silts and clays (i.e., < 63 μm) presented from all sites examined (Blott and Pye, 2001).

2.7. Radiocarbon dating and age-depth modelling

Accelerator mass spectrometry (AMS) radiocarbon (^{14}C) dating was carried out in the 14CHRONO Centre (Queen's University Belfast) to establish the chronostratigraphy of the cores from the Lothian, Gplot, Dhanchi, Dhanchi-2, and Sanekhali (see Table 1). Approximately 3 g of sediment was extracted for each of the samples for ^{14}C AMS radiocarbon dating. Each sample underwent pre-treatment involving an acid wash (HCl) to eliminate carbonates. Both bulk sediment and humic acid extraction was carried out for dating, with humic acid extraction methodology based on that of Lowe et al. (2004). All dates were calibrated against the IntCal13 curve (Reimer et al., 2013) with calibration carried out using the 'Clam' package by Blaauw (2020, 2010) in R Version 4.1.2 (Core Team, 2021). In order to derive rates of sedimentation for these sites, age-depth modelling through the 'Bacon' package in R was used to produce Bayesian age-depth models (Blaauw and Christen, 2011). Bacon calibrates ^{14}C dates against a specified ^{14}C calibration curve, which in this study was IntCal13. Bayesian age-depth modelling was utilised using default settings in Bacon, and these are summarised in Supplementary Figures B8-B11. Accumulation rates (mm yr^{-1}) are presented from the Lothian and Sajnekhali Island cores (see Fig. 7); three age-depth and accumulation models were produced for Sajnekhali due to the presence of age -reversals in the core. Age-depth modelling was not carried out on Dhanchi, Dhanchi-2, and Gplot due to numerous age-reversals and lack of dates. All Bayesian modelled dates are presented in Supplementary Tables C2-C5.

3. Results

3.1. Binomial logistic and beta regression GLM of TOC

The binomial logistic and beta regression models were applied to the TOC (prop.) and Al/Si data from Galy et al (2007) (see Supplementary Table 1). These input data consisted of surface sediments taken from Harding Bridge (n = 28), Sirajganj (n= 32), Mawa (n = 6), and Bhola (n = 13). The results from the binomial logistic regression GLM applied to the Galy et al. (2007) data are shown in Fig. 2, with a pseudo R^2 value of 0.76. Exploratory modeling revealed under-dispersion in the data (i.e. less variance in the outcome than expected). Here, the dispersion parameter was found to be 0.00019 indicating a high level of under-dispersion; a dispersion parameter of 1 suggests no under or over dispersion in the data. The model was therefore refitted using quasi-binomial distribution, which has no effect on the coefficient estimate, but in this case, reduced the standard errors (Zuur, 2009). We hypothesize that the primary cause of under-dispersion may be attributed to small sample values (Lord and Guikema, 2012; Sellers and Morris, 2017). The Beta regression is also presented (Fig. 3), with a pseudo R^2 of 0.82.

3.2. Predicted TOC from the Sundarbans

Predicted TOC from the Sundarbans plotted against depth are shown in Fig. 4. Median TOC in the sites ranged between 0.322% (IQR 0.269 – 0.445%) in Lothian; 0.320% (IQR 0.176 – 0.422%) in Gplot; 0.307% (IQR 0.256 – 0.354%) in Dhanchi; 0.275% (IQR 0.254 – 0.295%) in Dhanchi-2; 0.288% (IQR 0.267 – 0.363%) in Bonnie Camp; and 0.275% (IQR 0.244 – 0.319%) in Sajnekhali. The data from the Indian Sundarbans fall within the range of TOC values found in the Galy et al. (2007) data (i.e., median TOC at 0.46%, IQR: 0.275 – 0.575%, with a minimum and maximum range of 0.03% and 0.82%, respectively).

3.3. Grain-size analysis results from the Sundarbans

Median (D_{50}) grain-size from the Sundarbans are shown in Fig. 5 with grain size variability being composed predominately of the silt-sized fraction (4 – 63 μm), except for the Gplot core which has fine to medium sand. Grain-size data from the Sundarbans reveal an overwhelming majority of the sediment size fractions fall within the silt-size fraction (i.e., 4 – 63 μm) (Fig. 5). The limited grain size variability found in the Sundarbans is reflective of the homogeneous silts and clayey silts of most cores. The mud fraction (i.e., silt and clay, <63 um) is plotted against predicted TOC in the Sundarbans (Fig. 6) where a relatively strong relationship is found between mud and TOC in Lothian (Coefficient (Coef.) = –46.307; Standard Error (Std. E) = 4.793; p = <0.001; model R^2 = 0.56) and Dhanchi (Coef. = –60.265; Std. E = 6.502; p = <0.001; model R^2 = 0.55). A weaker relationship between mud and TOC is found in Dhanchi-2 (Coef. = –58.327; Std. E = 8.031; p = <0.001; model R^2 = 0.25) and Sajnekhali (Coef. = –35.613; Std. E = 4.559; p = <0.001; model R^2 = 0.26); with no discernible relationship found in Gplot (Coef. = –10.336; Std. E = 21.409; p = 0.636; model R^2 = 0.01) and Bonnie Camp (Coef. = –6.488; Std. E = 2.789; p = <0.05; model R^2 = 0.02). Linear regression of predicted TOC against depth for all sites (Fig. 7) showed there to be relatively strong correlations in Lothian (Coef. = –1460.09; Std. E = 96.00; p = <0.001; model R^2 = 0.74), Gplot (Coef. = –591.64; Std. E = 83.54; p = <0.001; model R^2 = 0.53) and Dhanchi (Coef. = –1776.96; Std. E = 239.68; p = <0.001; model R^2 = 0.44); with weaker correlations in Dhanchi-2 (Coef. = –1915.70; Std. E = 507.6; p = <0.001; model R^2 = 0.081), Bonnie Camp (Coef. = 1108.01; Std. E = 204.24; p = <0.001; model R^2 = 0.114), and Sajnekhali (Coef. = 655.41; Std. E = 238.96; p = <0.05; model R^2 = 0.041).

3.4. Radiocarbon (^{14}C) chronology

Table 1 shows the ^{14}C derived chronology from the Sundarbans; due to the nature of age-reversals in the Dhanchi and Dhanchi-2 core data, and the limited number of samples from Gplot (n = 2), further age-depth modelling was not carried out on these samples. LOESS-smoothed spline interpolation of the sedimentation rates (mm yr^{-1}) was plotted against depth for Lothian and Sajnekhali cores based on the Bayesian age-depth models (Supplementary Figures B9-B12) and these are presented in Fig. 8. The median sedimentation rate in Lothian was 1.67 mm yr^{-1} (IQR 1.25 – 2.00 mm yr^{-1}), with median sedimentation rates in Sajnekhali ranging from 1.25 – 2.00 mm yr^{-1}.

4. Discussion

4.1. Prediction of TOC from the Indian Sundarbans

Using the Al/Si and TOC quantification from Galy et al. (2007) as a 'calibration' dataset, we predicted TOC at six sites in the Sundarbans (this study) which revealed comparable levels of TOC to those reported by Galy et al. (2007). The overall range of predicted TOC would strongly indicate that terrestrial sources of organic matter (OM) are the main source of TOC in the Indian Sundarbans. It has been found that $\delta^{13}C$ compositions in the Sundarbans are comparable within the global range of mangroves and other coastal ecosystems (Prasad et al., 2017). Sedimentary OM is primarily influenced by terrestrial sources, particularly inputs from C_3 and C_4 metabolic plant pathways for both the Indian and Bangladeshi Sundarbans (Prasad et al., 2017). Plant litter, particulate, and suspended OM are sourced primarily from terrigenous matter, phytoplankton and marine particulates, as the dominant OM end-members in coastal ecosystems (Bala Krishna Prasad and Ramanathan, 2009; Gonneea et al., 2004; Prasad et al., 2017). For the first time (to the authors knowledge), the beta regression approach was used to model geochemical data, thus overcoming the challenges posed by compositional data, particularly the unit sum constraint. The advantages of the beta regression can also be seen in model flexibility in accounting for asymmetries in distributions and proportions; with Gaussian approaches found to be inaccurate in these respects (Cribari-Neto and Zeileis, 2010). Whilst Galy et al. (2007) used a linear regression model to fit the TOC and Al/Si data (Supplementary Figure 1), beta regression (Fig. 3) is the most appropriate approach to model “true” proportional data and its error structure (Cribari-Neto and Zeileis, 2010; Douma and Weedon, 2019).

4.2. TOC and grain-size variability in the Indian Sundarbans

There is a well-established relationship between grain size and OM, in that the OM of continental margin sediments increases concomitantly with finer grain size with clays (i.e., < 4 μm) found to have twice as much OM as silts (i.e., 4 – 63 μm), and four times as much OM as in fine sands (i.e., 63 – 250 μm), Trask (1939). The proposed mechanism for this relationship is the similarity of settling velocity (i.e., hydrodynamic or 'hydraulic' equivalence) of particulate OM and the fine-grained detrital minerals (Buchanan and Longbottom, 1970; Trask, 1939; Tyson, 1995). Furthermore, OM is also associated with TOC, with OC controlled by sediment properties, and/or impacted by mixing and sorting processes, similar to mixing and sorting of detrital grains (Galy et al., 2015, 2011, 2008, 2007). The results here show that grain-size data from the Sundarbans reveal an overwhelming majority of the sediment size fractions fall within the silt-size fraction (i.e., 4 – 63 μm), reflective of the homogeneous silts and clayey silts characterised for the surface sediments of the lower western tide-dominated delta plain, compared to that found on the eastern fluvial-dominated delta (Allison et al., 2003). Thus, hydrodynamic conditions, and sediment grain size, play a determinant role in the deposition of OM and associated TOC (Tyson, 1995). We observed results in agreement with this interpretation at Lothian and Dhanchi. However, the relationship was less clear at Dhanchi-2 and Sajnekhali, and was not observed at all in the Bonnie Camp and Gplot data. We hypothesise that between-site differences could be driven by various processes of mixing of sand mud fractions under complex hydrodynamic processes within the Indian Sundarbans (*cf.,* Venkatramanan et al., 2013). We posit that this complex mixing process may be site specific, given the overall variability of predicted TOC with depth (Fig. 7). Notwithstanding this variation, our predicted TOC results are in relative agreement with previous studies (Allison et al., 2003), with reported ranges from 0.05% to 1.1%.

We argue that the variation of D_{50} grain size and TOC in the Indian Sundarbans may reflect a number of non-mutually exclusive processes. Our data primarily support the explanation that the observed between-site differences may reflect the increasingly reworked nature of the sediments (Allison et al., 2003; Flood et al., 2018; Rogers et al., 2013). Sediments in the Sundarbans are considered to be reworked from G-B sourced muds from the delta front (*cf.,* Allison et al., 2003; Rogers et al., 2013), and are understood to be delivered through onshore advection during monsoonal and cyclonic coastal setup events (*cf.,* Allison and Kepple, 2001; Flood et al., 2018). TOC is both inversely correlated with sand content and the sand-mud ratio (*cf.,* Bornhold and Yorath, 1984; Syvitski et al., 1990; Tyson, 1995) and TOC may also be inversely correlated with mean size of the silt fraction (Scheidegger and Krissek, 1983; Tyson, 1995). In contemporary sediments the maximum level of TOC is generally better correlated with grain size than in the minimum TOC fraction (Gross, 1967; Romankevich and Shirshov, 2013; Tyson, 1995). The correlation between grain size and TOC may partly reflect the greater surface area of finer particles, in a form of sediment-specific surface area (*cf.,* Tyson, 1995, pp. 87), which is related to the amount of organic carbon that may be absorbed on sediment surfaces (Hedges et al., 1993; Keil and Hedges, 1993). Alternatively, it is known that downcore decreases in TOC content are indicative of rapid sediment respiration rates with burial (Allison et al., 2003). In the active progradational lower delta plain sediments, TOC preservation is low, relative to marsh and mangrove deposits in the more inactive delta complex (Allison et al., 2003).

Alternative explanations for temporal variability in TOC throughout the Sundarbans may be related to the influence of seasonal fluctuations between saline flooding and rainwater flushing (Allison et al., 2003). Strong differences associated with poorer drainage and organic preservation are found to coincide with higher OM preservation in parts of the Sundarbans that tend to dry out between annual floods (Kosters, 1989; J. M. Coleman, 1966; Allison et al., 2003). In the Sundarbans sediments OM breakdown is facilitated by the relatively high permeability of the silt-dominated sequence (*cf.,* Allison et al., 2003). Lastly, Tidal morphodynamics play a significant role in the determination of sediment balance within an estuarine system, primarily channel geometry in the form of channel convergence into funnel planimetric shape and sloping characteristics of the bed, and the degree of sinuosity; these morphodynamic factors control tide propagation along the channel (Lanzoni and Seminara, 2002). Net sediment transport, in terms of magnitude and direction, over the course of a tidal cycle, affects the tidal asymmetry, leading to unequal duration and/or unequal magnitude of ebb and flood tides (Dronkers, 1986; Lanzoni and Seminara, 2002; Townend and Pethick, 2002). Tidal flow asymmetries that are characterized in the form of shorter flood duration and higher flood current maximum (i.e., flood dominance) will lead to landward directed sediment transport; with shorter fall periods and greater ebb current (i.e., ebb dominance) leading to net seaward directed sediment transport (Dronkers, 1986; Lanzoni and Seminara, 2002; Townend and Pethick, 2002). Whilst it is not yet clear, morphodyamic process may be influencing the observations at Bonnie Camp and Sajnekhali.

4.3. Sedimentation rates and burial of TOC

The inconsistency of ^{14}C ages throughout the sites dated in the Indian Sundarbans (Table 1) likely reveals a complicated sedimentary environment (*cf.,* Nian et al., 2018). The introduction of old C may have taken place with sediment storage and reworking along the dispersal path from the delta plain to delta mouth as a main cause of older dates and age reversals (*cf.,* Stanley and Chen, 2000). Self-cannibalisation of tidally-deposited sediments is understood to be most important in the Sundarbans, particularly in the eastern delta complex with regards reworking of sediments (Allison, 1998b; Woodroffe, 2010). Radiocarbon dates of the Holocene sequence of the Indian Sundarbans need to be complimented with a multi-method geochronological approach, such as optically stimulated luminescence (OSL) dating quartz silt (Chamberlain et al., 2017). Although tidally reworked sediments, may prove too challenging for OSL dating (Chamberlain et al., 2017). The assessment of the uncertainties involved in the reconstruction of the sedimentation rates from the Indian Sundarbans is both dynamic and complex, and highlights the limitations of ^{14}C dating methods in this environment (*cf.,* Nian et al., 2018).

The Indian Sundarbans however is considered to be sediment starved, eroding, and cut-off from major distributary sources of sediment (Flood et al., 2018). Estimates of mid-late Holocene sedimentation on the most eastern extent of the tidal delta plain in Bangladesh reveal mean rates of ∼1.1 cm yr^{-1}, with accretion attributed to a mix of flood pulse sediment and reworking of older sediments from the shelf or tidal channel beds (Allison and Kepple, 2001; Rogers et al., 2013). Accretion rates due to this net sedimentation are approximately equal to the mean regional rate of relative sea-level rise (RSLR) of ∼1.0 cm yr^{-1} (Rogers et al., 2013). Accretion is complicated by varying estimates of subsidence rates (i.e., increasing water level) across the delta plain at c. ~3.0 mm yr^{-1} (Becker et al., 2020, and references therein).

The sedimentation rate in the Sundarbans is higher during the wet monsoon season (i.e., June-October), with greater frequency and deeper inundation of island sites carrying suspended sediment loads (Hale et al., 2019). The primary future challenge facing the Indian Sundarbans is the sustainable delivery of sediment and accretion in the tide-dominated mangrove sites (Hale et al., 2019). Reduction in mangrove areas worldwide in recent decades may have consequences for OM exchange at the land-ocean boundary (Jennerjahn and Ittekkot, 2002). In the case of the Sundarbans, possible worst-case scenarios for reduced sediment delivery range between 14–18%, along with an increase in the duration of the dry season (i.e., November-May) by one month or more has the potential to reduce overall sediment deposition by approximately half of what is presently observed (Hale et al., 2019). Such a worst-case scenario results in a sedimentation rate that is below the rate of local sea level rise (*cf.,* Hale et al., 2019), resulting in a threat to the continued viability of the Sundarbans as a sustainable form of C burial. The successful burial of atmospheric C in the Sundarbans is predicated on the successful accretion and sustainability of sediment delivery which at present looks more precarious.

5. Conclusions

In this study we explored the variation of TOC in the Indian Sundarbans from six cores collected from five sites. The main study findings are:

(1) The data from Galy et al. (2007) in combination with the beta regression modelling approach, has given reliable predictions for TOC for the Indian Sundarbans. TOC has varied across sites, with accumulation rates coincident with accretion across sites.

(2) Radiocarbon (^{14}C) dating has shown the variability of sedimentation rates over the last 5,000 years; with sedimentation found to be greatest at Sajnekhali relative to Lothian – with uncertainty of ^{14}C dates associated with the reworked nature of delta sediments found in this study.

(3) Variation in TOC over the last 5,000 years has illustrated the role of sediment depositional processes in controlling TOC burial, with TOC found to accumulate alongside decreasing grain-size. The observed between-site differences reflecting the increasingly reworked nature of the sediments associated with tidal advection as the primary driver of TOC delivery.

The study has found that TOC burial and sedimentation are intimately related in the Indian Sundarbans, but with TOC burial reliant on the sustainable delivery of detrital sediment to island sites, future rates of TOC will be ultimately predicated on successful retention of tidal sedimentation in the context of flood risk management using embankments to resist further marine incursions on inhabited tidal islands (Adnan et al., 2020).

Acknowledgements

RPF and JDO would like to acknowledge the support and assistance of Vincent van Walt and Van Walt Environmental Ltd., in the core extraction and research support; and would also like to acknowledge the logistical support in the Sundarbans provided through the Institute of

Environmental Studies & Wetland Management (IESWM), Kolkata, West Bengal, India. RPF would like to acknowledge the support of the 14CHRONO Centre for Climate, the Environment, and Chronology, Queen's University of Belfast (QUB) for facilitating radiocarbon dating of samples used in this study. RPF and JDO would like to thank John Pethick for our discussions on tidal morphodynamics in the Sundarbans. RPF would like to acknowledge the support of Laois County Council (ROI) and the Department of Employment and Learning (NI) in their administration of PhD funding support.

Author contributions

RPF developed the study concept, JDO obtained funding for field work, RPF and JDO carried out field work jointly, and RPF carried out all laboratory analyses as part of PhD study. MGM developed the binomial logistic and beta regression methods for TOC prediction. GTS carried out Bayesian age-depth modelling and manuscript review; IDB edited figures and manuscript text for publication. The first manuscript draft was written by RPF and revised by all co-authors. All authors contributed to the intellectual content expressed herein.

Declaration of Competing Interest

The authors declare that there is no conflict of interest.

References

Adnan, M.S.G., Talchabhadel, R., Nakagawa, H., Hall, J.W., 2020. How much of the south western delta of Bangladesh can be restored with Tidal River Management (TRM)? Science of The Total Environment 138747. https://doi.org/10.1016/j.scitotenv.2020.138747

Allison, M., Kepple, E., 2001. Modern sediment supply to the lower delta plain of the Ganges-Brahmaputra River in Bangladesh. Geo-Mar Lett 21, 66–74. https://doi.org/10.1007/s003670100069

Allison, M.A., 1998a. Geologic framework and environmental status of the Ganges-Brahmaputra delta. J. Coast. Res. 14, 826–836.

Allison, M.A., 1998b. Historical Changes in the Ganges-Brahmaputra Delta Front. Journal of Coastal Research 14, 1269–1275.

Allison, M.A., Khan, S.R., Goodbred, S.L., Kuehl, S.A., 2003. Stratigraphic evolution of the late Holocene Ganges–Brahmaputra lower delta plain. Sedimentary Geology, Sedimentary Geology of the Bengal Basin, Bangladesh, in relation to the Asia-Greater

India collision and the evolution of the eastern Bay of Bengal 155, 317–342. https://doi.org/10.1016/S0037-0738(02)00185-9

Alongi, D.M., 2012. Carbon sequestration in mangrove forests. Carbon Management 3, 313–322. https://doi.org/10.4155/cmt.12.20

Aucour, A.-M., France-Lanord, C., Pedoja, K., Pierson-Wickmann, A.-C., Sheppard, S.M.F., 2006. Fluxes and sources of particulate organic carbon in the Ganga-Brahmaputra river system. Global Biogeochemical Cycles 20. https://doi.org/10.1029/2004GB002324

Bala Krishna Prasad, M., Ramanathan, A.L., 2009. Organic matter characterization in a tropical estuarine-mangrove ecosystem of India: Preliminary assessment by using stable isotopes and lignin phenols. Estuarine, Coastal and Shelf Science 84, 617–624. https://doi.org/10.1016/j.ecss.2009.07.029

Becker, M., Papa, F., Karpytchev, M., Delebecque, C., Krien, Y., Khan, J.U., Ballu, V., Durand, F., Le Cozannet, G., Islam, A.K.M.S., Calmant, S., Shum, C.K., 2020. Water level changes, subsidence, and sea level rise in the Ganges–Brahmaputra–Meghna delta. Proc Natl Acad Sci USA 117, 1867–1876. https://doi.org/10.1073/pnas.1912921117

Blaauw, M., 2020. clam: Classical Age-Depth Modelling of Cores from Deposits.

Blaauw, M., 2010. Methods and code for ‘classical’ age-modelling of radiocarbon sequences. Quaternary Geochronology 5, 512–518. https://doi.org/10.1016/j.quageo.2010.01.002

Blaauw, M., Christen, J.A., 2011. Flexible paleoclimate age-depth models using an autoregressive gamma process. Bayesian Anal. 6, 457–474. https://doi.org/10.1214/11-BA618

Blott, S.J., Pye, K., 2001. GRADISTAT: a grain size distribution and statistics package for the analysis of unconsolidated sediments. Earth Surf. Process. Landforms 26, 1237–1248. https://doi.org/10.1002/esp.261

Bornhold, B.D., Yorath, C.J., 1984. Surficial geology of the continental shelf, northwestern Vancouver Island. Marine Geology 57, 89–112. https://doi.org/10.1016/0025-3227(84)90196-8

Bouillon, S., Borges, A.V., Castañeda-Moya, E., Diele, K., Dittmar, T., Duke, N.C., Kristensen, E., Lee, S.Y., Marchand, C., Middelburg, J.J., Rivera-Monroy, V.H., Smith, T.J., Twilley, R.R., 2008. Mangrove production and carbon sinks: A revision of global budget estimates. Global Biogeochemical Cycles 22. https://doi.org/10.1029/2007GB003052

Bu, N.-S., Qu, J.-F., Li, G., Zhao, B., Zhang, R.-J., Fang, C.-M., 2015. Reclamation of coastal salt marshes promoted carbon loss from previously-sequestered soil carbon pool. Ecological Engineering 81, 335–339. https://doi.org/10.1016/j.ecoleng.2015.04.051

Buchanan, J.B., Longbottom, M.R., 1970. The determination of organic matter in marine muds: The effect of the presence of coal and the routine determination of protein. Journal of Experimental Marine Biology and Ecology 5, 158–169. https://doi.org/10.1016/0022-0981(70)90014-6

Butman, D., Stackpoole, S., Stets, E., McDonald, C.P., Clow, D.W., Striegl, R.G., 2016. Aquatic carbon cycling in the conterminous United States and implications for terrestrial carbon accounting. PNAS 113, 58–63. https://doi.org/10.1073/pnas.1512651112

Callaway, J.C., Borgnis, E.L., Turner, R.E., Milan, C.S., 2012. Carbon Sequestration and Sediment Accretion in San Francisco Bay Tidal Wetlands. Estuaries and Coasts 35, 1163–1181. https://doi.org/10.1007/s12237-012-9508-9

Chamberlain, E.L., Wallinga, J., Reimann, T., Goodbred, S.L., Steckler, M.S., Shen, Z., Sincavage, R., 2017. Luminescence dating of delta sediments: Novel approaches explored for the Ganges-Brahmaputra-Meghna Delta. Quaternary Geochronology 41, 97–111. https://doi.org/10.1016/j.quageo.2017.06.006

Chmura, G.L., Anisfeld, S.C., Cahoon, D.R., Lynch, J.C., 2003. Global carbon sequestration in tidal, saline wetland soils. Global Biogeochemical Cycles 17. https://doi.org/10.1029/2002GB001917

Coleman, J.M., 1966. Ecological Changes in Massive Fresh-Water Clay Sequence: ABSTRACT. Bulletin 50. https://doi.org/10.1306/5D25B737-16C1-11D7-8645000102C1865D

Core Team, R., 2021. R: A Language and Environment for Statistical Computing. R Foundation for Statistical Computing, Vienna.

Cribari-Neto, F., Zeileis, A., 2010. Beta Regression in *R*. J. Stat. Soft. 34. https://doi.org/10.18637/jss.v034.i02

Crooks, S., Emmett-Mattox, S., Findsen, J., 2010. Findings of the National Blue Ribbon Panel on the Development of a Greenhouse Gas Offset Protocol for Tidal Wetlands Restoration and Management: action plan to guide protocol development: Restore America's Estuaries. Philip Williams & Associates, Ltd., and Science Applications International Corporation.

Douma, J.C., Weedon, J.T., 2019. Analysing continuous proportions in ecology and evolution: A practical introduction to beta and Dirichlet regression. Methods in Ecology and Evolution 10, 1412–1430. https://doi.org/10.1111/2041-210X.13234

Dronkers, J., 1986. Tidal asymmetry and estuarine morphology. Netherlands Journal of Sea Research 20, 117–131. https://doi.org/10.1016/0077-7579(86)90036-0

Duarte, C.M., Marbà, N., Gacia, E., Fourqurean, J.W., Beggins, J., Barrón, C., Apostolaki, E.T., 2010. Seagrass community metabolism: Assessing the carbon sink capacity of seagrass meadows. Global Biogeochemical Cycles 24. https://doi.org/10.1029/2010GB003793

Duarte, C.M., Middelburg, J.J., Caraco, N., 2005. Major role of marine vegetation on the oceanic carbon cycle. Biogeosciences 2, 1–8. https://doi.org/10.5194/bg-2-1-2005

Dutta, M.K., Bianchi, T.S., Mukhopadhyay, S.K., 2017. Mangrove Methane Biogeochemistry in the Indian Sundarbans: A Proposed Budget. Front. Mar. Sci. 4. https://doi.org/10.3389/fmars.2017.00187

Emmett-Mattox, S., Crooks, S., Findsen, J., 2011. Gases and grasses: The restoration, conservation, or avoided loss of tidal wetlands carbon pools may help mitigate climate change. Environ.Forum 28, 30–35.

Ferrari, S., Cribari-Neto, F., 2004. Beta Regression for Modelling Rates and Proportions. Journal of Applied Statistics 31, 799–815. https://doi.org/10.1080/0266476042000214501

Flood, R.P., 2014. Post Mid-Holocene Sedimentation of the West Bengal Sundarbans (Ph.D. thesis). Queen's University Belfast, Belfast.

Flood, R.P., Barr, I.D., Weltje, G.J., Roberson, S., Russell, M.I., Meneely, J., Orford, J.D., 2018. Provenance and depositional variability of the Thin Mud Facies in the lower Ganges-Brahmaputra delta, West Bengal Sundarbans, India. Marine Geology 395, 198–218. https://doi.org/10.1016/j.margeo.2017.09.001

Flood, R.P., Bloemsma, M.R., Weltje, G.J., Barr, I.D., O'Rourke, S.M., Turner, J.N., Orford, J.D., 2016. Compositional data analysis of Holocene sediments from the West Bengal Sundarbans, India: Geochemical proxies for grain-size variability in a delta environment. Applied Geochemistry 75, 222–235. https://doi.org/10.1016/j.apgeochem.2016.06.006

Flood, R.P., Orford, J.D., McKinley, J.M., Roberson, S., 2015. Effective grain size distribution analysis for interpretation of tidal–deltaic facies: West Bengal Sundarbans. Sedimentary Geology 318, 58–74. https://doi.org/10.1016/j.sedgeo.2014.12.007

France-Lanord, C., Derry, L.A., 1997. Organic carbon burial forcing of the carbon cycle from Himalayan erosion. Nature 390, 65–67. https://doi.org/10.1038/36324

Freedman, B., Stinson, G., Lacoul, P., 2009. Carbon credits and the conservation of natural areas. Environ. Rev. 17, 1–19. https://doi.org/10.1139/A08-007

Galy, V., Eglinton, T., 2011. Protracted storage of biospheric carbon in the Ganges–Brahmaputra basin. Nature Geosci 4, 843–847. https://doi.org/10.1038/ngeo1293

Galy, V., France-Lanord, C., Beyssac, O., Faure, P., Kudrass, H., Palhol, F., 2007. Efficient organic carbon burial in the Bengal fan sustained by the Himalayan erosional system. Nature 450, 407–410. https://doi.org/10.1038/nature06273

Galy, V., France-Lanord, C., Beyssac, O., Lartiges, B., Rhaman, M., 2011. Organic Carbon Cycling During Himalayan Erosion: Processes, Fluxes and Consequences for the Global Carbon Cycle, in: Lal, R., Sivakumar, M.V.K., Faiz, S.M.A., Mustafizur Rahman, A.H.M., Islam, K.R. (Eds.), Climate Change and Food Security in South Asia. Springer Netherlands, Dordrecht, pp. 163–181. https://doi.org/10.1007/978-90-481-9516-9_12

Galy, V., France-Lanord, C., Lartiges, B., 2008. Loading and fate of particulate organic carbon from the Himalaya to the Ganga–Brahmaputra delta. Geochimica et Cosmochimica Acta 72, 1767–1787. https://doi.org/10.1016/j.gca.2008.01.027

Galy, V., Peucker-Ehrenbrink, B., Eglinton, T., 2015. Global carbon export from the terrestrial biosphere controlled by erosion. Nature 521, 204–207. https://doi.org/10.1038/nature14400

Gonneea, M.E., Paytan, A., Herrera-Silveira, J.A., 2004. Tracing organic matter sources and carbon burial in mangrove sediments over the past 160 years. Estuarine, Coastal and Shelf Science 61, 211–227. https://doi.org/10.1016/j.ecss.2004.04.015

Goodbred, S.L., Kuehl, S.A., 2000. The significance of large sediment supply, active tectonism, and eustasy on margin sequence development: Late Quaternary stratigraphy and evolution of the Ganges–Brahmaputra delta. Sedimentary Geology 133, 227–248. https://doi.org/10.1016/S0037-0738(00)00041-5

Gross, M.G., 1967. Organic carbon in surface sediment from the northeast Pacific Ocean. International Journal of Oceanology and Limnology 1, 46–54.

Guisan, A., Edwards, T.C., Hastie, T., 2002. Generalized linear and generalized additive models in studies of species distributions: setting the scene. Ecological Modelling 157, 89–100. https://doi.org/10.1016/S0304-3800(02)00204-1

Hale, R.P., Wilson, C.A., Bomer, E.J., 2019. Seasonal Variability of Forces Controlling Sedimentation in the Sundarbans National Forest, Bangladesh. Front. Earth Sci. 7. https://doi.org/10.3389/feart.2019.00211

Hansen, L.T., 2009. The Viability of Creating Wetlands for the Sale of Carbon Offsets. Journal of Agricultural and Resource Economics 34, 350–365.

Hedges, J.I., Keil, R.G., Cowie, G.L., 1993. Sedimentary diagenesis: organic perspectives with inorganic overlays. Chemical Geology 107, 487–492. https://doi.org/10.1016/0009-2541(93)90237-D

Hotchkiss, E.R., Jr, R.O.H., Sponseller, R.A., Butman, D., Klaminder, J., Laudon, H., Rosvall, M., Karlsson, J., 2015. Sources of and processes controlling CO 2 emissions change with the size of streams and rivers. Nature Geosci 8, 696–699. https://doi.org/10.1038/ngeo2507

Iacono, C.L., Mateo, M.A., Gràcia, E., Guasch, L., Carbonell, R., Serrano, L., Serrano, O., Dañobeitia, J., 2008. Very high-resolution seismo-acoustic imaging of seagrass meadows (Mediterranean Sea): Implications for carbon sink estimates. Geophysical Research Letters 35. https://doi.org/10.1029/2008GL034773

Jennerjahn, T.C., Ittekkot, V., 2002. Relevance of mangroves for the production and deposition of organic matter along tropical continental margins. Naturwissenschaften 89, 23–30. https://doi.org/10.1007/s00114-001-0283-x

Keil, R.G., Hedges, J.I., 1993. Sorption of organic matter to mineral surfaces and the preservation of organic matter in coastal marine sediments. Chemical Geology 107, 385–388. https://doi.org/10.1016/0009-2541(93)90215-5

Kennedy, H., Beggins, J., Duarte, C.M., Fourqurean, J.W., Holmer, M., Marbà, N., Middelburg, J.J., 2010. Seagrass sediments as a global carbon sink: Isotopic constraints. Global Biogeochemical Cycles 24. https://doi.org/10.1029/2010GB003848

Kosters, E.C., 1989. Organic-clastic Facies Relationships and Chronostratigraphy of the Barataria Interlobe Basin, Mississippi Delta Plain. SEPM JSR Vol. 59. https://doi.org/10.1306/212F8F2B-2B24-11D7-8648000102C1865D

Laffoley, D.D., Grimsditch, G.D., Great Britain, IUCN World Commission on Protected Areas (Eds.), 2009. The management of natural coastal carbon sinks. IUCN, Gland, Switzerland.

Lanzoni, S., Seminara, G., 2002. Long-term evolution and morphodynamic equilibrium of tidal channels. Journal of Geophysical Research: Oceans 107, 1-1-1–13. https://doi.org/10.1029/2000JC000468
Lord, D., Guikema, S.D., 2012. The Conway–Maxwell–Poisson model for analyzing crash data. Applied Stochastic Models in Business and Industry 28, 122–127. https://doi.org/10.1002/asmb.937
Lowe, J.J., Walker, M.J.C., Scott, E.M., Harkness, D.D., Bryant, C.L., Davies, S.M., 2004. A coherent high-precision radiocarbon chronology for the Late-glacial sequence at Sluggan Bog, Co. Antrim, Northern Ireland. Journal of Quaternary Science 19, 147–158. https://doi.org/10.1002/jqs.814
Luisetti, T., Turner, R.K., Andrews, J.E., Jickells, T.D., Kröger, S., Diesing, M., Paltriguera, L., Johnson, M.T., Parker, E.R., Bakker, D.C.E., Weston, K., 2019. Quantifying and valuing carbon flows and stores in coastal and shelf ecosystems in the UK. Ecosystem Services 35, 67–76. https://doi.org/10.1016/j.ecoser.2018.10.013
Mcleod, E., Chmura, G.L., Bouillon, S., Salm, R., Björk, M., Duarte, C.M., Lovelock, C.E., Schlesinger, W.H., Silliman, B.R., 2011. A blueprint for blue carbon: toward an improved understanding of the role of vegetated coastal habitats in sequestering CO2. Frontiers in Ecology and the Environment 9, 552–560. https://doi.org/10.1890/110004
Nellemann, C. (Christian), Corcoran, E., Duarte, C.M., Valdes, L., DeYoung, C., Fonseca, L., Grimsditch, G.D., 2009. Blue carbon : the role of healthy oceans in binding carbon : a rapid response assessment.
Nian, X., Zhang, W., Wang, Z., Sun, Q., Chen, J., Chen, Z., Hutchinson, S.M., 2018. The chronology of a sediment core from incised valley of the Yangtze River delta: Comparative OSL and AMS 14C dating. Marine Geology 395, 320–330. https://doi.org/10.1016/j.margeo.2017.11.008
Prasad, M.B.K., Kumar, A., Ramanathan, A.L., Datta, D.K., 2017. Sources and dynamics of sedimentary organic matter in Sundarban mangrove estuary from Indo-Gangetic delta. Ecological Processes 6, 8. https://doi.org/10.1186/s13717-017-0076-6
Regnier, P., Friedlingstein, P., Ciais, P., Mackenzie, F.T., Gruber, N., Janssens, I.A., Laruelle, G.G., Lauerwald, R., Luyssaert, S., Andersson, A.J., Arndt, S., Arnosti, C., Borges, A.V., Dale, A.W., Gallego-Sala, A., Goddéris, Y., Goossens, N., Hartmann, J., Heinze, C., Ilyina, T., Joos, F., LaRowe, D.E., Leifeld, J., Meysman, F.J.R., Munhoven, G., Raymond, P.A., Spahni, R., Suntharalingam, P., Thullner, M., 2013. Anthropogenic perturbation of the carbon fluxes from land to ocean. Nature Geosci 6, 597–607. https://doi.org/10.1038/ngeo1830
Reimer, P.J., Bard, E., Bayliss, A., Beck, J.W., Blackwell, P.G., Ramsey, C.B., Buck, C.E., Cheng, H., Edwards, R.L., Friedrich, M., Grootes, P.M., Guilderson, T.P., Haflidason, H., Hajdas, I., Hatté, C., Heaton, T.J., Hoffmann, D.L., Hogg, A.G., Hughen, K.A., Kaiser, K.F., Kromer, B., Manning, S.W., Niu, M., Reimer, R.W., Richards, D.A., Scott, E.M., Southon, J.R., Staff, R.A., Turney, C.S.M., Plicht, J. van der, 2013. IntCal13 and Marine13 Radiocarbon Age Calibration Curves 0–50,000 Years cal BP. Radiocarbon 55, 1869–1887. https://doi.org/10.2458/azu_js_rc.55.16947
Rogers, K.G., Goodbred, S.L., Mondal, D.R., 2013. Monsoon sedimentation on the ‘abandoned’ tide-influenced Ganges–Brahmaputra delta plain. Estuarine, Coastal and Shelf Science 131, 297–309. https://doi.org/10.1016/j.ecss.2013.07.014
Romankevich, E.A., Shirshov, P., 2013. Geochemistry of Organic Matter in the Ocean. Springer Berlin / Heidelberg, Berlin, Heidelberg.
Sarkar, A., Sengupta, S., McArthur, J.M., Ravenscroft, P., Bera, M.K., Bhushan, R., Samanta, A., Agrawal, S., 2009. Evolution of Ganges–Brahmaputra western delta plain: Clues from sedimentology and carbon isotopes. Quaternary Science Reviews 28, 2564–2581. https://doi.org/10.1016/j.quascirev.2009.05.016
Scheidegger, K.F., Krissek, L.A., 1983. Zooplankton and Nekton: Natural Barriers to the Seaward Transport of Suspended Terrigenous Particles off Peru, in: Suess, E., Thiede, J. (Eds.), Coastal Upwelling Its Sediment Record. Springer US, Boston, MA, pp. 303–333. https://doi.org/10.1007/978-1-4615-6651-9_16

Scott, D.N., Wohl, E.E., 2017. Evaluating carbon storage on subalpine lake deltas. Earth Surface Processes and Landforms 42, 1472–1481. https://doi.org/10.1002/esp.4110

Sellers, K.F., Morris, D.S., 2017. Underdispersion models: Models that are “under the radar.” Communications in Statistics - Theory and Methods 46, 12075–12086. https://doi.org/10.1080/03610926.2017.1291976

Stanley, D.J., Chen, Z., 2000. Radiocarbon Dates in China’s Holocene Yangtze Delta: Record of Sediment Storage and Reworking, Not Timing of Deposition. Journal of Coastal Research 16, 8.

Stocker, T.F., Qin, D., Plattner, G.-K., Tignor, M.M.B., Allen, S.K., Boschung, J., Nauels, A., Xia, Y., Bex, V., Midgley, P.M., 2013. Working Group I Contribution to the Fifth Assessment Report of the Intergovernmental Panel on Climate Change 14.

Subramanian, V., Ittekot, V., 1991. Carbon transport by the Himalayan Rivers. Carbon transport by the Himalayan Rivers 157–168.

Sutfin, N.A., Wohl, E.E., Dwire, K.A., 2016. Banking carbon: a review of organic carbon storage and physical factors influencing retention in floodplains and riparian ecosystems. Earth Surface Processes and Landforms 41, 38–60. https://doi.org/10.1002/esp.3857

Syvitski, J.P.M., LeBlanc, K.W.G., Cranston, R.E., 1990. The flux and preservation of organic carbon in Baffin Island fjords. Geological Society, London, Special Publications 53, 177–199. https://doi.org/10.1144/GSL.SP.1990.053.01.10

Townend, I., Pethick, J., 2002. Estuarine flooding and managed retreat. Philosophical Transactions of the Royal Society of London. Series A: Mathematical, Physical and Engineering Sciences 360, 1477–1495. https://doi.org/10.1098/rsta.2002.1011

Trask, P., 1939. Organic content of recent sediments. A Symposium. Am. Assoc. Petro. Geol 11, 428–452.

Tyson, R.V., 1995. Sedimentary Organic Matter. Springer Netherlands, Dordrecht. https://doi.org/10.1007/978-94-011-0739-6

Venkatramanan, S., Ramkumar, T., Anithamary, I., 2013. Distribution of grain size, clay mineralogy and organic matter of surface sediments from Tirumalairajanar Estuary, Tamilnadu, east coast of India. Arab J Geosci 6, 1371–1380. https://doi.org/10.1007/s12517-011-0423-3

Wagner, W., Lague, D., Mohrig, D., Passalacqua, P., Shaw, J., Moffett, K., 2017. Elevation change and stability on a prograding delta: Change and Stability on Prograding Delta. Geophys. Res. Lett. https://doi.org/10.1002/2016GL072070

Watanabe, K., Kuwae, T., 2015. How organic carbon derived from multiple sources contributes to carbon sequestration processes in a shallow coastal system? Glob Chang Biol 21, 2612–2623. https://doi.org/10.1111/gcb.12924

Weltje, G.J., Tjallingii, R., 2008. Calibration of XRF core scanners for quantitative geochemical logging of sediment cores: Theory and application. Earth and Planetary Science Letters 274, 423–438. https://doi.org/10.1016/j.epsl.2008.07.054

Wickham, H., 2016. ggplot2: Elegant Graphics for Data Analysis. Springer-Verlag, New York.

Woodroffe, C.D., 2010. Assessing the Vulnerability of Asian Megadeltas to Climate Change Using GIS, in: Green, D.R. (Ed.), Coastal and Marine Geospatial Technologies, Coastal Systems and Continental Margins. Springer Netherlands, Dordrecht, pp. 379–391. https://doi.org/10.1007/978-1-4020-9720-1_36

Yang, S.L., Luo, X., Temmerman, S., Kirwan, M., Bouma, T., Xu, K., Zhang, S., Fan, J., Shi, B., Yang, H., Wang, Y.P., Shi, X., Gao, S., 2020. Role of delta-front erosion in sustaining salt marshes under sea-level rise and fluvial sediment decline: Role of delta-front erosion in sustaining marsh. Limnol Oceanogr. https://doi.org/10.1002/lno.11432

Zuur, A.F. (Ed.), 2009. Mixed effects models and extensions in ecology with R, Statistics for biology and health. Springer, New York, NY.

List of figures

Fig. 1. Location of the Ganges-Brahmaputra Delta, with inlay map showing location of Hardinge Bridge (Ganges), Sirajganj (Brahmaputra), Mawa, and Bhola (Lower Meghna) sampled by Galy et al. (2007), with Lothian, Gplot, Dhanchi, Dhanchi-2, Bonnie Camp, and Sajnekhali (this study).

Fig. 2. Binomial logistic regression GLM applied to Galy et al. (2007) TOC (prop.) and ln(Al/Si) data with 95% CI ribbon. Pseudo R^2 value of the binomial logistic regression GLM = 0.76.

Fig. 3. Beta regression (pseudo R^2 value of beta regression = 0.82) with quantiles (2.25% and 97.5% plotted as a ribbon around model). As a result of the beta distribution, on which the model predictions are made, being skewed (i.e., the data are fitted to the beta distribution to account for the fact that they cannot be >1.0 or <0.0), standard deviation and confidence intervals used in linear models cannot be used here; instead quantiles of the predicted beta distribution are used here to show the predicted range of values.

Fig. 4. Predicted TOC in percentage format (%) from; (a) Lothian, (b) Gplot, (c) Dhanchi, (d) Dhanchi-2, (e) Bonnie Camp, and (f) Sajnekhali (beta regression model coefficients used).

Fig. 5. Median grain-size (D_{50} μm) from: (a) Lothian, (b) Gplot, (c) Dhanchi, (d) Dhanchi-2, (e) Bonnie Camp, and (f) Sajnekhali. The overall median grain size in Lothian was 38.12 μm (IQR 32.69 – 42.05 μm), Gplot at 92.18 μm (IQR 31.44 – 151.49 μm), Dhanchi at 28.19 μm (IQR 25.69 – 31.58 μm), Dhanchi-2 at 31.23 μm (IQR 28.27 – 32.62 μm), Bonnie Camp at 31.60 μm (IQR 30.32 – 32.73 μm), and Sajnekhali at 33.39 μm (IQR 31.26 – 35.86 μm).

Fig. 6. Linear regression of how predicted TOC changes with median size fraction for all sites (blue line), where D_{50} < 63 µm; (a) Lothian, (b) Gplot, (c) Dhanchi, (d) Dhanchi-2, (e) Bonnie Camp, (f) Sajnekhali; a trend of increasing TOC with decreasing size is found (a, c, d, f) with no strong relationship found in two sites (b & e).

Fig. 7. Linear regression of predicted TOC against depth for all sites (blue line); (a) Lothian, (b) Gplot, (c) Dhanchi, (d) Dhanchi-2, (e) Bonnie Camp, (f) Sajnekhali; a trend of increasing TOC is found from the bottom to the top of cores (a-d), and a decreasing TOC trend from the bottom to the top of cores (e & f).

Fig. 8. LOESS-smoothed spline interpolation of sedimentation rates (mm yr^{-1}) for Lothian (a) and Sajnekhali (b-d) based on Bayesian age-depth model. The median sedimentation rate (mm yr^{-1}) in Lothian is 1.67 mm yr^{-1} (IQR 1.25 – 2.00 mm yr^{-1}). Three age-depth models (Supplementary Figures B9, B10, B11) were carried out on Sajnekhali due to the presence of age-reversals; median sedimentation rates range from 2.00 mm yr^{-1} (IQR 1.43 – 2.16 mm yr^{-1}) (b), 2.00 mm yr^{-1} (IQR 1.43 – 2.50 mm yr^{-1}) (c), 1.25 mm yr^{-1} (IQR 1.00 – 2.50 mm yr^{-1}) (d).

List of tables

Table 1: ^{14}C chronology from the Sundarbans.

Appendix A. Supplementary material

Supplementary Material A1. R Markdown for Estuarine-deltaic controls on coastal carbon burial in the western Ganges-Brahmaputra delta over the last 5,000 years (HTML).

Supplementary Material A2. R Markdown for Estuarine-deltaic controls on coastal carbon burial in the western Ganges-Brahmaputra delta over the last 5,000 years (PDF).

Supplementary Material A3. R Markdown Code for Supplementary Material A1, A2 (RMD File).

Supplementary Table A4. Sundarbans Al/Si data file used in Supplementary Material A3 (.csv file).

Supplementary Table A5. TOC data from Galy et al. (2007) used in Supplementary Material A3 (.csv file).

Appendix B. Supplementary figures

Supplementary Figure B1. TOC for sediments of the Ganges (filled blue symbols), the Brahmaputra (filled green symbols), Lower Meghna (filled orange symbols) as a function of Al/Si (Galy et al., 2007). A positive linear relationship (R2 = 0.89, $p \leq 0.001$) with sediments from all three rivers having a similar positive trend between TOC and Al/Si, indicative of similar OC loadings (Galy et al., 2007). In sandy and quartz-enriched bed sediments, TOC is found to be very low (circles); TOC linearly increases with the relative proportion of aluminium-enriched fine-grained minerals found in the suspended sediments (squares) (Galy et al., 2007). Sediments from the three rivers show a comparable positive trend, indicative of the similar OC loading relative to their composition (Galy et al., 2007). Best fit (solid black line) and 95% confidence interval (CI: dashed black lines) are shown in the figure (after Galy et al., 2007).

Supplementary Figure B2. Median grain-size (D_{50} µm) from: (a) Lothian, (b) Gplot, (c) Dhanchi, (d) Dhanchi-2, (e) Bonnie Camp, and (f) Sajnekhali.

Supplementary Figure B3. < 63 µm grain-size fraction from: (a) Lothian, (b) Gplot, (c) Dhanchi, (d) Dhanchi-2, (e) Bonnie Camp, and (f) Sajnekhali.

Supplementary Figure B4. Linear regression of how predicted TOC changes with median size fraction (D_{50}) for all sites (blue line); (a) Lothian (R^2 = 0.54), (b) Gplot (R^2 = 0.52), (c) Dhanchi (R^2 = 0.55), (d) Dhanchi-2 (R^2 = 0.25), (e) Bonnie Camp (R^2 = 0.02), (f) Sajnekhali (R^2 = 0.05).

Supplementary Figure B5. Relationship between the TOC and clay fraction (< 4 µm) for all sites; (a) Lothian, (b) Gplot, (c) Dhanchi, (d) Dhanchi-2, (e) Bonnie Camp, (f) Sajnekhali.

Supplementary Figure B6. Relationship between the TOC and silt fraction (4 – 64 μm) for all sites; (a) Lothian, (b) Gplot, (c) Dhanchi, (d) Dhanchi-2, (e) Bonnie Camp, (f) Sajnekhali.

Supplementary Figure B7. Relationship between the TOC and mud (i.e., silt and clay fraction, < 63 μm) for all sites; (a) Lothian, (b) Gplot, (c) Dhanchi, (d) Dhanchi-2, (e) Bonnie Camp, (f) Sajnekhali.

Supplementary Figure B8. Linear regression of predicted TOC against depth for all sites; Lothian (R^2 = 0.74), Gplot (R^2 = 0.53), Dhanchi (R^2 = 0.44), Dhanchi-2 (R^2 = 0.08), Bonnie Camp (R^2 = 0.11), Sajnekhali (R^2 = 0.04); Lothian, Gplot, Dhanchi, and Dhanchi-2 show a trend with rising TOC towards core surfaces, with Bonnie Camp and Sajnekhali showing reverse trends in predicted TOC values.

Supplementary Figure B9. Bayesian age-depth models constructed with the 'Bacon' age-depth modelling package in R for Lothian Island core ^{14}C dates. Bayesian age-depth modelling utilised default settings within 'Bacon' (i.e., a piece-wise linear model with 5 cm sections, a gamma prior for sedimentation rate with a mean of 20 and shape 1.5, a beta prior for memory with mean of 0.7 and strength of 4, and a student-t distribution to deal with outlying dates). All modelled dates are presented in Supplementary Table 2. The grayscale on the model represents the likelihood, where darker gray indicates the greater likelihood that the model ran through that section of the core. The top panel shows three plots for each model: the left panel plot shows the model stability; the middle plot shows the prior (green line) and posterior (gray filled) distributions of accumulation mean; and the panel plot on the right shows the prior (green line) and posterior (gray filled) distributions of memory properties.

Supplementary Figure B10. Bayesian age-depth model constructed with the 'Bacon' age-depth modelling package in R for Sajnekhali Island core. All ^{14}C dates from Sajnekhali (see Table 1) were included in this model run. Mean 95% confidence ranges 380 yr, min. 61 yr at 0 cm, max. 506 yr at 145 cm; 62% of the dates overlap with the age-depth model (95% ranges). All modelled dates are presented in Supplementary Table 3.

Supplementary Figure B11. Bayesian age-depth models constructed with the 'Bacon' age-depth modelling package in R for Sajnekhali Island core. This model run was performed on a subset of ^{14}C dates from Sajnekhali (i.e., UBA-22971, UBA-22968, UBA-22967, UBA-22966, see Table 1). Mean 95% confidence ranges 514 yr, min. 58 yr at 0 cm, max. 701 yr at 275 cm 100% of the dates overlap with the age-depth model (95% ranges). All modelled dates are presented in Supplementary Table 4.

Supplementary Figure B12. Bayesian age-depth models constructed with the 'Bacon' age-depth modelling package in R for Sajnekhali Island core. This model run was performed on a subset of ^{14}C dates from Sajnekhali (i.e., UBA-22972, UBA-22970, UBA-22969, see Table 1). Mean 95% confidence ranges 558 yr, min. 57 yr at 0 cm, max. 724 yr at 180 cm, with 75% of the dates overlap with the age-depth model (95% ranges). All modelled dates are presented in Supplementary Table 5.

Appendix C. Supplementary tables

Supplementary Table C1: Total suspended sediment (TSS), Al/Si, TOC and of river sediments and gravels from Galy et al. (2007); Al/Si and TOC data used in beta regression model.

Supplementary Table C2: Lothian Bacon Bayesian age-depth model interpolated calibrated ages (input data for Supplementary Figure B9).

Supplementary Table C3: Sajnekhali Bacon Bayesian age-depth model interpolated calibrated ages (input data for Supplementary Figure B10).

Supplementary Table C4: Sajnekhali Bacon Bayesian age-depth model interpolated calibrated ages (input data for Supplementary Figure B11).

Supplementary Table C5: Sajnekhali Bacon Bayesian age-depth model interpolated calibrated ages (input data for Supplementary Figure B12).

Supplementary Table C6: Outputs from binomial logistic regression GLM of Galy et al. (2007) TOC and ln(Al/Si) data used in Fig. 3 (main text).

Supplementary Table C7: Outputs from beta regression GLM of Galy et al. (2007) TOC and ln(Al/Si) data used in Fig. 4 (main text).

Supplementary Table C8: Predicted TOC data from the Indian Sundarbans sites (i.e., from Lothian, Gplot, Dhanchi, Dhanchi-2, Bonnie Camp, and Sajnekhali) used in Fig. 4 and Fig. 7 (main text).

Supplementary Table C9: Median grain size (D_{50} μm) and predicted TOC from beta regression from the Indian Sundarbans sites (i.e., from Lothian, Gplot, Dhanchi, Dhanchi-2, Bonnie Camp, and Sajnekhali) used in Fig. 5 and Fig. 6 (main text).

Supplementary Table C10: Grain size data in quarter phi (φ) intervals from the Indian Sundarbans sites (i.e., from Lothian, Gplot, Dhanchi, Dhanchi-2, Bonnie Camp, and Sajnekhali).

Supplementary Table C11: X-ray flourescence (XRF) geochemical composition from the Indian Sundarbans sites (i.e., from Lothian, Gplot, Dhanchi, Dhanchi-2, Bonnie Camp, and Sajnekhali); Al and Si elemental ratios used in this study.

Figure 1

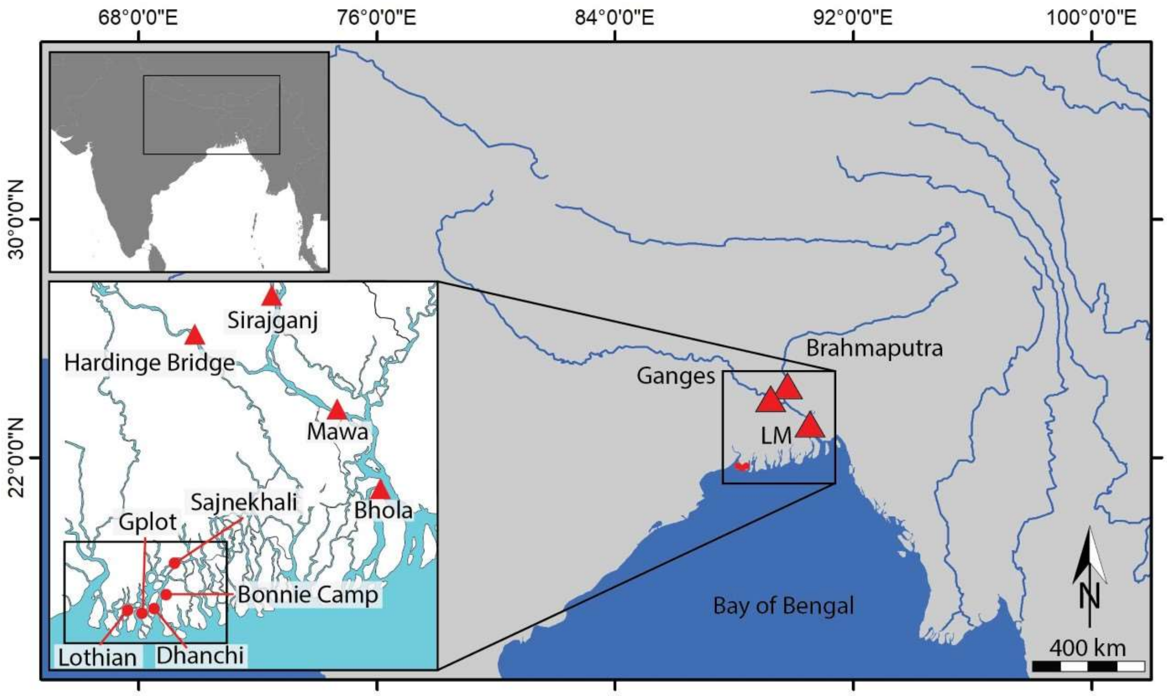

68°0'0"E
76°0'0"E
84°0'0"E
92°0'0"E
100°0'0"E
30°0'0"N
22°0'0"N
Sirajganj
Hardinge Bridge
Mawa
Bhola
Sajnekhali
Gplot
Bonnie Camp
Lothian
Dhanchi
Brahmaputra
Ganges
LM
Bay of Bengal
N
400 km

Figure 2

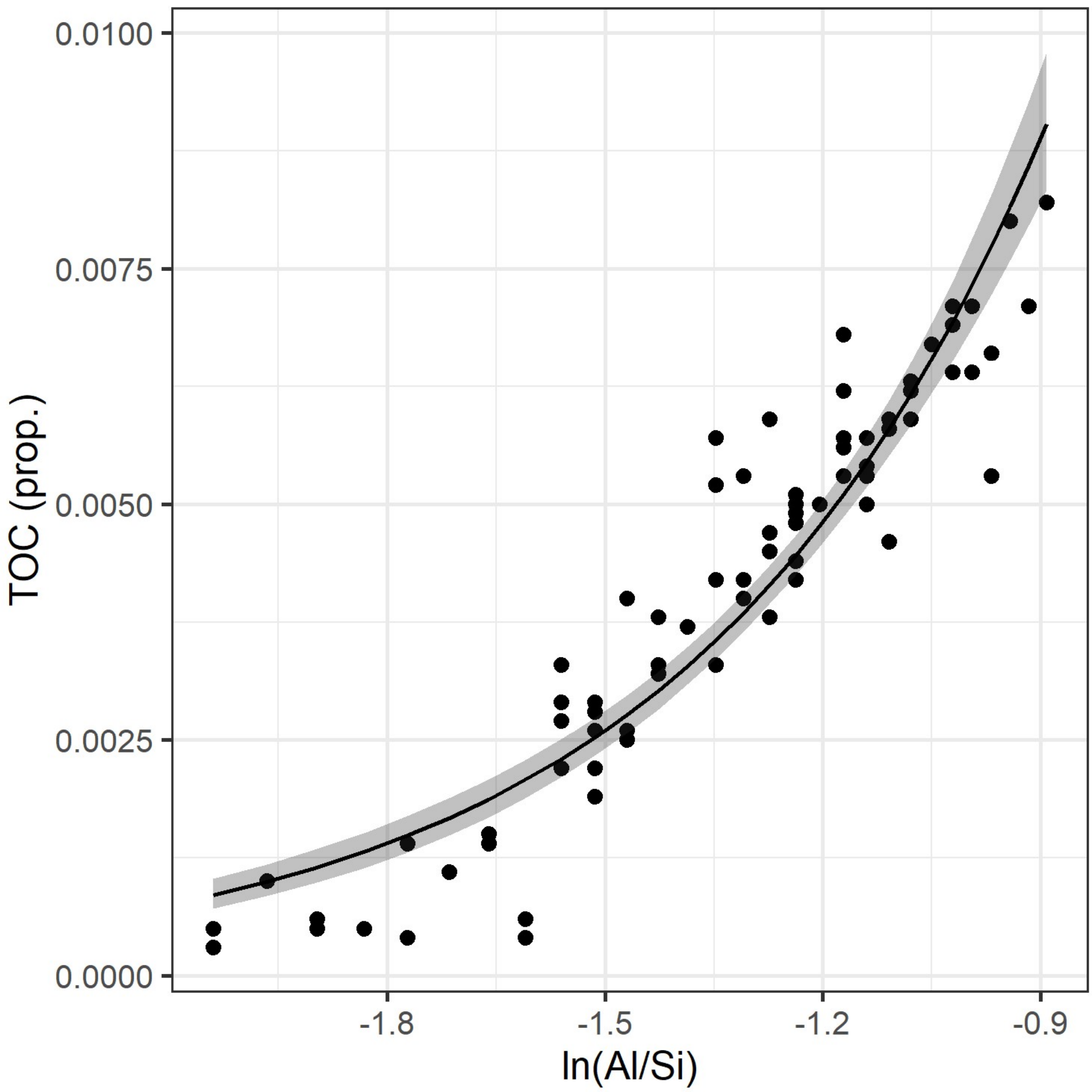

Figure 3

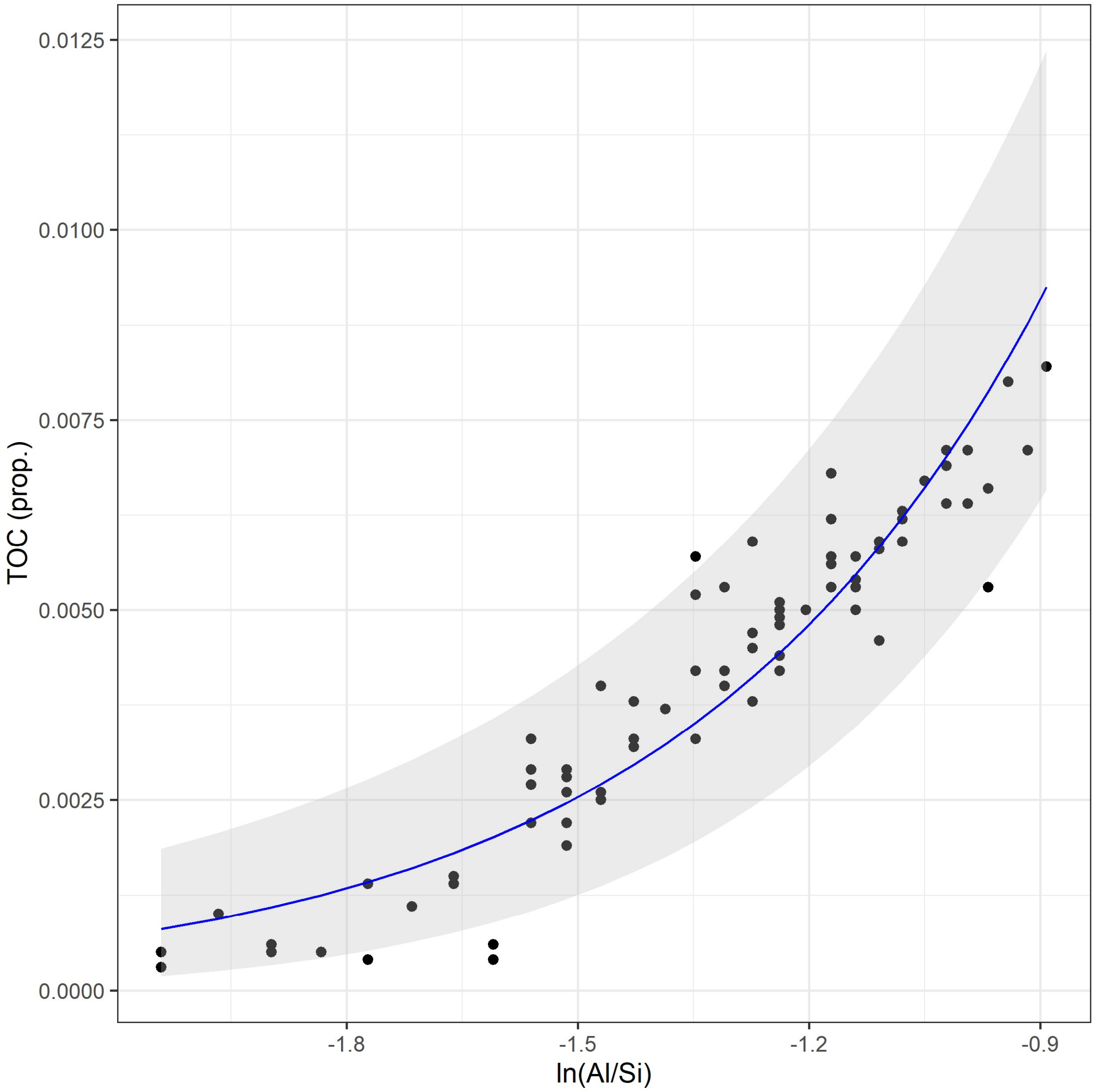

0.0125
0.0100
0.0075
0.0050
0.0025
0.0000
TOC (prop.)
-1.8
-1.5
-1.2
-0.9
ln(Al/Si)

Figure 4

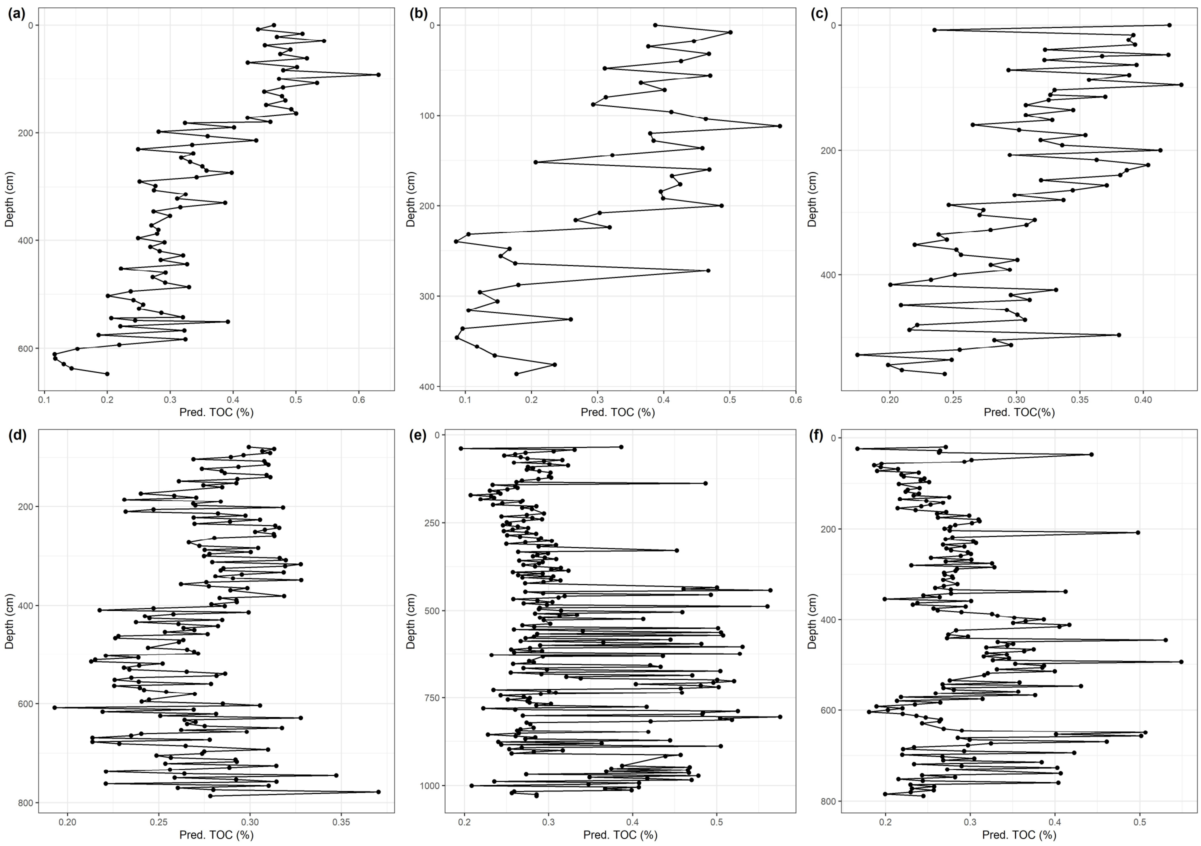

(a)
Depth (cm)
Pred. TOC (%)
(b)
Depth (cm)
Pred. TOC (%)
(c)
Depth (cm)
Pred. TOC(%)
(d)
Depth (cm)
Pred. TOC (%)
(e)
Depth (cm)
Pred. TOC (%)
(f)
Depth (cm)
Pred. TOC (%)

Figure 5

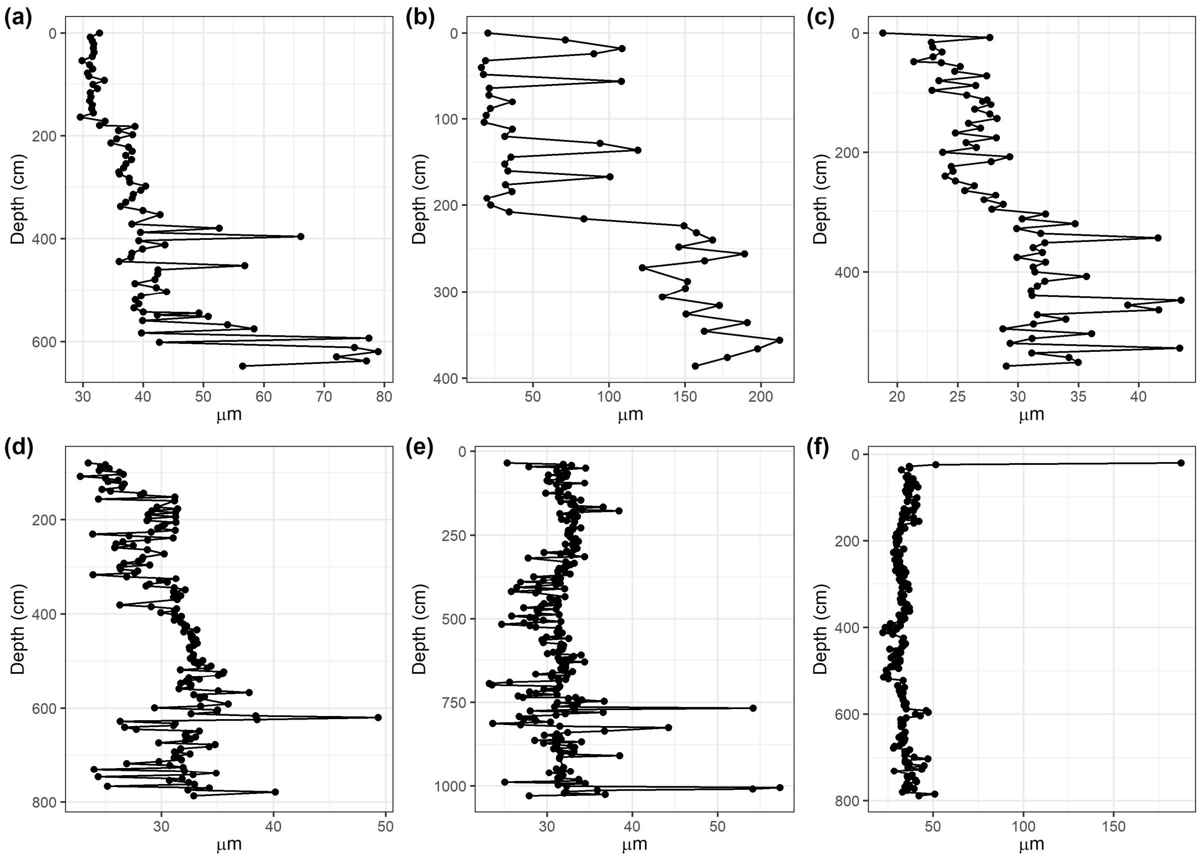

Figure 6

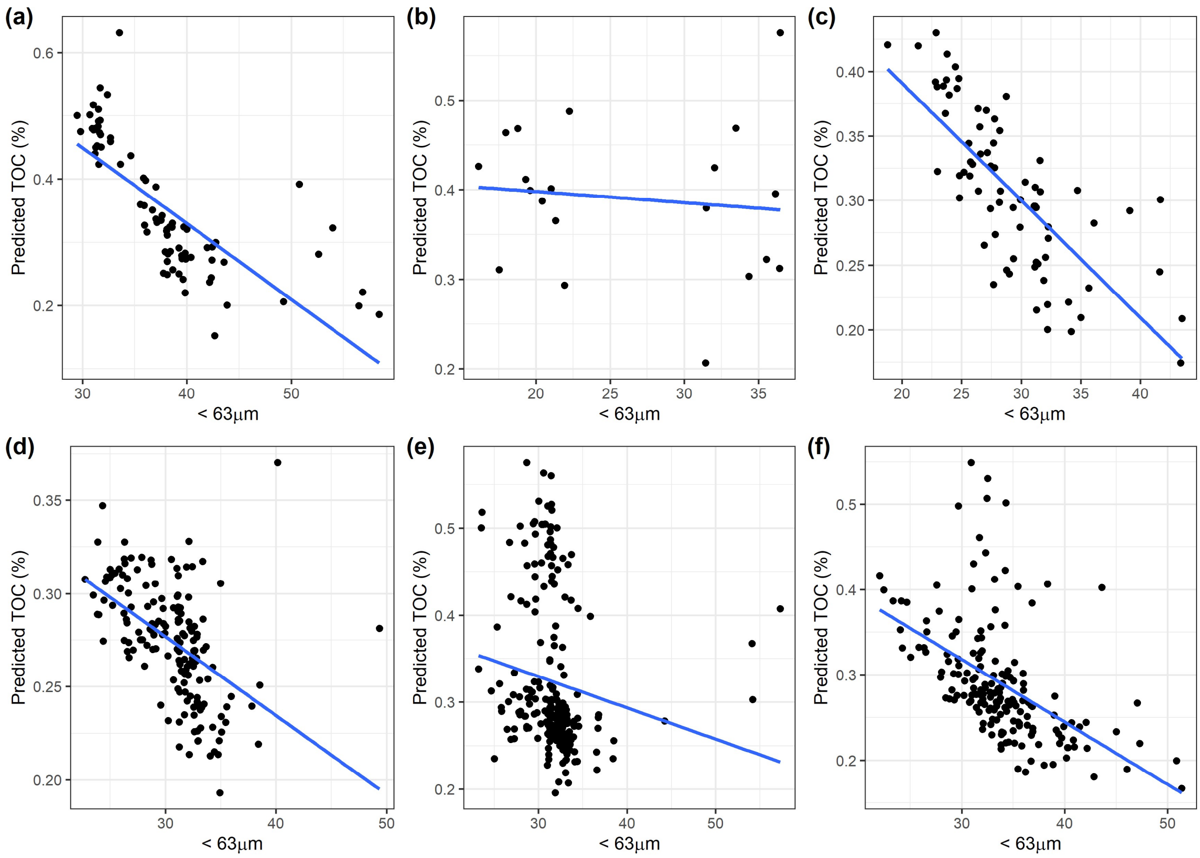

Figure 7

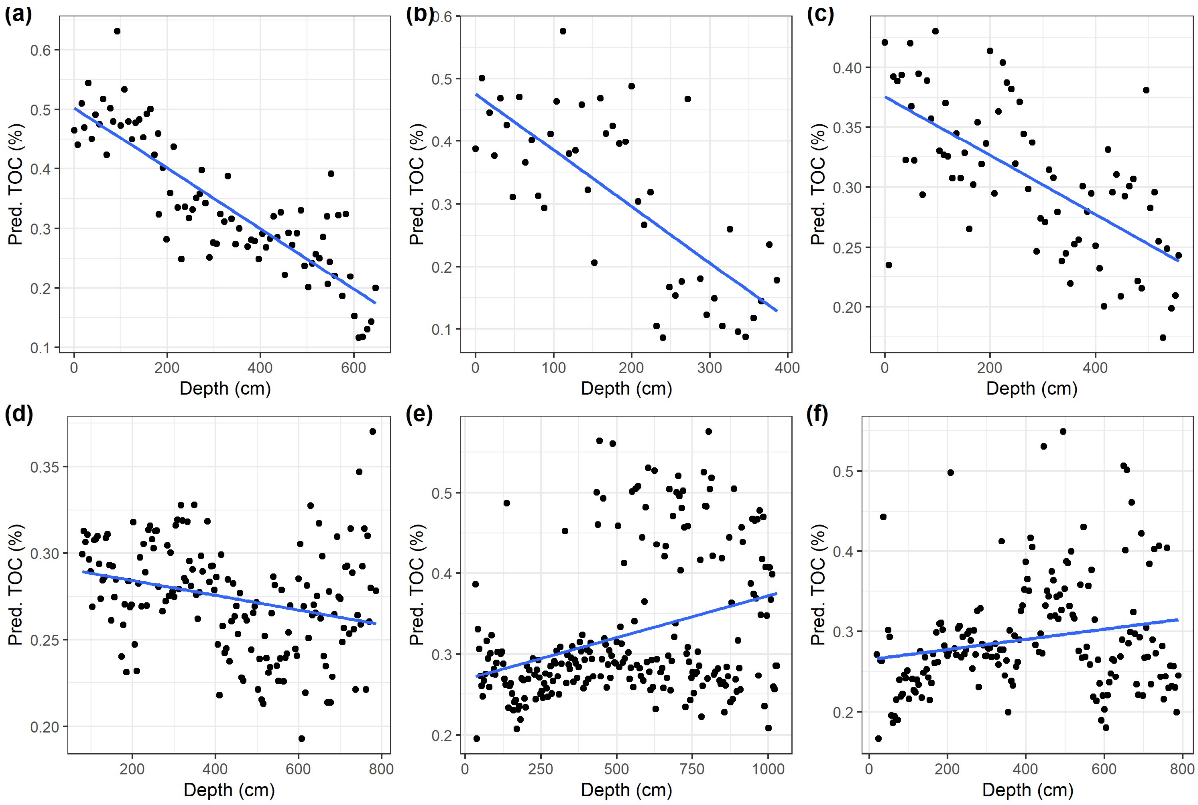

(a)
Pred. TOC (%)
0.6
0.5
0.4
0.3
0.2
0.1
0
200
400
600
Depth (cm)
(b)
0.6
0.5
0.4
0.3
0.2
0.1
0
100
200
300
400
(c)
0.40
0.35
0.30
0.25
0.20
(d)
0.35
0.30
0.25
0.20
800
(e)
250
500
750
1000
(f)

Figure 8

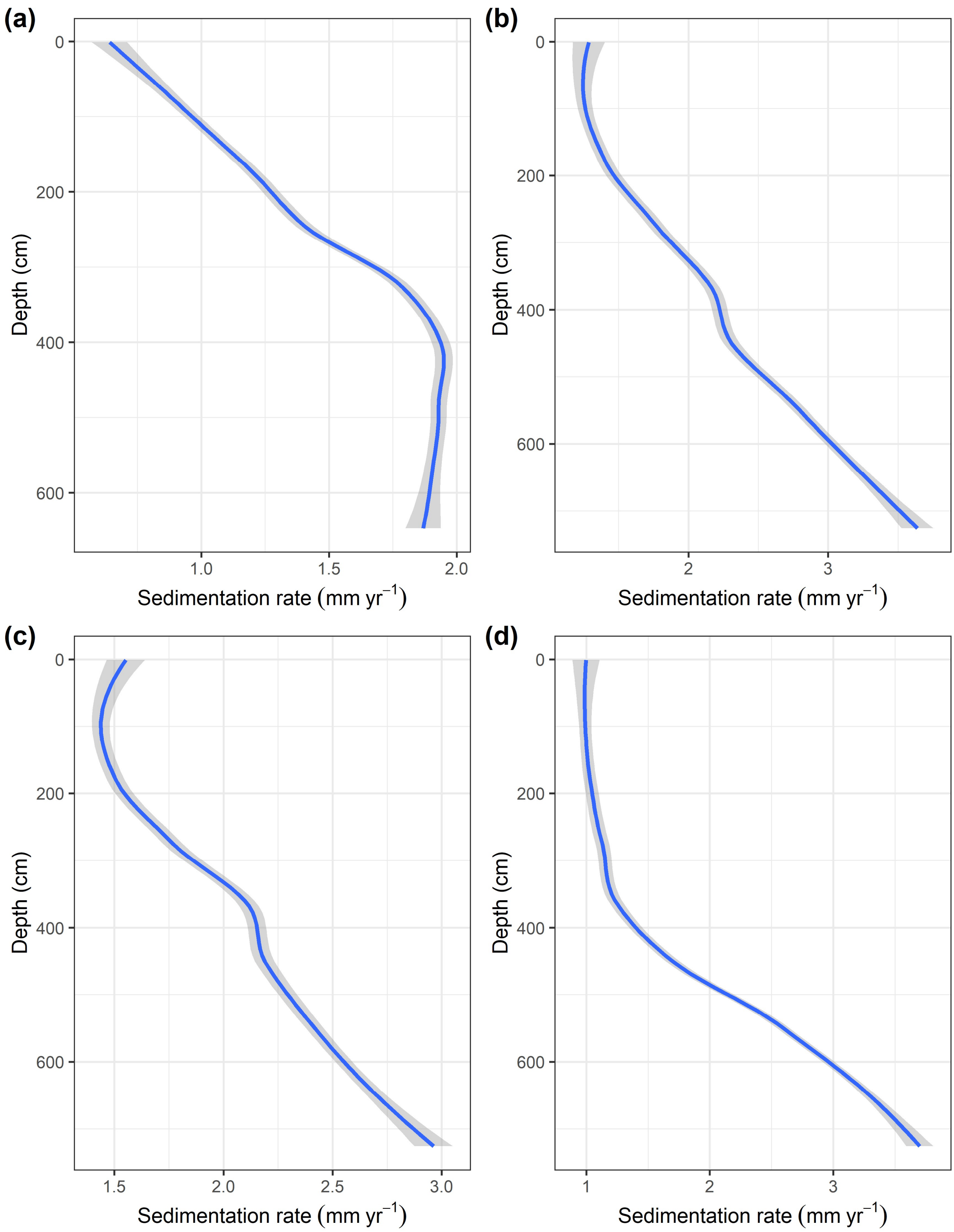

(a)
0
200
400
600
Depth (cm)
1.0
1.5
2.0
Sedimentation rate (mm yr−1)
(b)
0
200
400
600
Depth (cm)
2
3
Sedimentation rate (mm yr−1)
(c)
0
200
400
600
Depth (cm)
1.5
2.0
2.5
3.0
Sedimentation rate (mm yr−1)
(d)
0
200
400
600
Depth (cm)
1
2
3
Sedimentation rate (mm yr−1)

Table 1

Site	ID	Depth (cm)	^{14}C age (±2σ)	Calendar age with 2σ error (cal yr BP)	Material
Lothian	Surface	0		-60*	NA
	UBA-20910	70	1271 ±25	1277-1178	Humic acid
	UBA-20571	164	1868 ±28	1873-1727	Humic acid
	UBA-20569	214	2409 ±39	2698-2347	Humic acid
	UBA-21170	274	2868 ±49	3155-2865	Humic acid
	UBA-18154	647	4291 ±35	4959-4826	Bulk sediment
Gplot	Surface	0		-60*	
	UBA-18992	184	4291 ±37	4961-4826	Bulk sediment
	UBA-18993	224	3383 ±37	3719-3510	Bulk sediment
Dhanchi	Surface	0		-60*	
	UBA-21040	78	2635 ±34	2841-2724	Humic acid
	UBA-21039	158	1620 ±28	1565-1414	Humic acid
	UBA-20908	160	2777 ±33	2951-2790	Humic acid
	UBA-21038	214	1437 ±34	1384-1294	Humic acid
	UBA-18989	280	4245 ±36	4867-4649	Bulk sediment
	UBA-18991	512	4528 ±40	5312-5047	Bulk sediment
	UBA-18152	558	4081 ±26	4801-4447	Bulk sediment
Dhanchi-2	Surface	0		-61**	
	UBA-23517	137.5	3281 ±35	3586-3409	Humic acid
	UBA-23516	239	2585 ±34	2769-2519	Humic acid
	UBA-23515	335	2438 ±31	2700-2357	Humic acid
	UBA-23514	433	3127 ±37	3444-3240	Humic acid
	UBA-23513	530	3070 ±48	3383-3161	Humic acid
	UBA-23512	628	2815 ±40	3055-2798	Humic acid
	UBA-23511	725	2596 ±38	2782-2518	Humic acid
Sajnekhali	Surface	0		-61**	NA
	UBA-22973	86	ND	ND	Humic acid
	UBA-22972	185	2991 ±35	3328-3063	Humic acid
	UBA-22971	283	2205 ±30	2316-2146	Humic acid
	UBA-22970	383	3356 ±40	3692-3481	Humic acid
	UBA-22969	479	3562 ±44	3974-3721	Humic acid
	UBA-22968	577	3249 ±35	3561-3397	Humic acid
	UBA-22967	673.5	3356 ±37	3690-3482	Humic acid
	UBA-22966	726	3389 ±33	3707-3563	Humic acid

Date of sample retrieval 2010* and 2011**. ND: No data.